

A MECHANISM OF SOUND GENERATION FROM VORTEX PREDOMINANT FLOWS

Igor Men'shov, Yoshiaki Nakamura
*Nagoya University

Keywords: *vortex flow, instability, sound generation*

Abstract

The present paper addresses the vortex instability as a possible source mechanism of wake vortex sound. We study a family of circular planar vortices that have zero total circulation, with the swirl velocity being presented by a generalized Taylor-type distribution in the radial direction. The vortex is assumed to be compressible and homentropic; its azimuthal velocity is characterized by two parameters: intensity μ that is proportional to the maximal velocity and "steepness" β that defines the typical scale of the opposite vorticity zone surrounding the core of the vortex. The linear analysis is conducted to investigate the evolution of normal mode disturbances imposed on the field of the basic flow. Results obtained concern the effect of the parameters μ and β on instability characteristics. The far field analysis shows that the instability evolution in the linear stage is accompanied by radiation of monochromatic sound waves with the frequency that equals the phase frequency of the unstable mode. Also included are results of the numerical simulation of the non-linear stage, which is related to the vortex breakdown and subsequent sound emission.

1 Introduction

Vortex motion is a dominant property of wake flows. Resulted from instability of shear layers, large vortical structures are created in the wake and travel downstream. These structures commonly reveal unstable behavior that eventually

can lead to the well-known phenomenon of vortex breakdown. Therefore, a mechanism that can be suggested as a possible source of aerodynamic sound in the wake flow is the presence of instabilities within the vortex itself, their evolution, and as a result, the vortex breakdown. The question we address in the present paper is the sound that emitted in the far field because of these phenomena.

Just as an illustration to the foregoing, we show some results of one calculation in Fig. 1. This is the direct numerical simulation of the $M_\infty = 0.12$ compressible viscous flow past a fence-type obstacle. In the figure, the flow is represented by instantaneous pressure (Fig. 1a) and velocity divergence (Fig. 1b) distributions. The pressure field reveals large vortical structures that appear in the flow behind the obstacle. The velocity divergence, which actually represents small fluctuations of density because of the effect of compressibility, clearly shows that these vortices are destabilized as they propagate downstream and acquire a typical 4-leafed structure. One can also see that the vortex destabilization is accompanied by the radiation of sound waves (Fig. 1b).

If the vortex were two-dimensional and monotonic with one-signed vorticity (finite non-zero circulation), it has been shown [1] that it would be stable by the Rayleigh criteria. However, real wake vortices actually have more complicated structure. In particular, they may include an annulus of opposite vorticity that surrounds the core so that the circulation around the vortex vanishes with the radial direction [2]. A strong shear layer just behind the core characterizes the

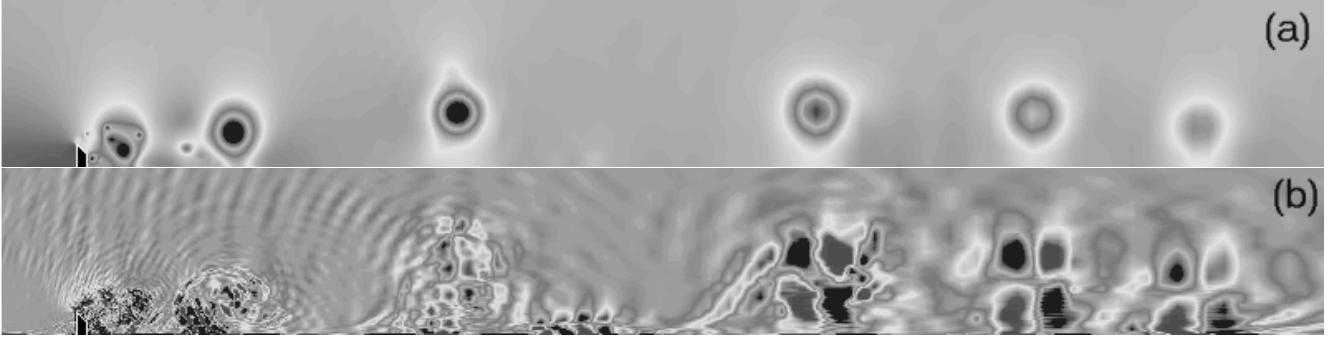


Fig. 1 Results of DNS for air flow with a Mach number $M_\infty = 0.12$ past a fence obstacle. (a) pressure field; (b) velocity divergence field.

distribution of the azimuthal velocity in such vortices, which can be destabilized and trigger the vortex instability.

The family of vortices with zero total circulation was introduced in [3] and now referred to as isolated vortices. For isolated vortices, the circulation vanishes at a finite distance from the core depending on a single parameter, the steepness β . In the present paper, we adopt the model of isolated vortex to simulate the wake vortices, and proceed to the stability analysis to obtain temporal instability characteristics and investigate the asymptotic behavior of disturbances in the far field.

There are lots of investigations have been carried out to the present day, which are devoted to the stability of isolated vortices. Most of these studies concern the model of incompressible fluid. The evolution of two-dimensional perturbations in an axisymmetric vortex was studied in [3], where the instability was found that results in the formation of multipolar vortex structures like tripoles and quadrupoles. It also was shown that the azimuthal shear is the major mechanism of the multipolar formation and that the order of the multipole depends on the steepness of the velocity distribution in the opposite vorticity region surrounding the vortex core ([4] and [5]). The three-dimensional instability of isolated vortices was studied in [6] by the direct numerical simulation of the linear impulse response. The results of this study showed that whereas the axisymmetric mode is the most unstable mode (the centrifugal

instability), yet larger azimuthal modes are also destabilized as the steepness of the opposite vorticity zone is increased.

The focus of the present paper is to investigate the effect of compressibility on the stability of isolated vortices with the emphasis on the sound that is resulted in the far field from the instability development in the basic vortex. The paper is organized into 2 parts. First, the linear-stability analysis is performed to determine unstable normal modes and their quantitative characteristics - the growth rate and azimuthal phase velocity. These parameters govern the asymptotic behavior of eigenfunctions in the far field, which just represent the sound from the instability. Second, the numerical calculation of the Navier-Stokes equations is carried out to simulate the non-linear stage of the instability development that involves the vortex destruction and its decay into child vortical structures.

2 Linear-Stability Analysis

2.1 Formulation

We consider the two-dimensional equations governing the motion of a nondissipative compressible fluid in polar coordinates (r, ϕ) . We will use conventional notations ρ , u , v , p , s , c to denote the density, radial and azimuthal components of the velocity vector, pressure, entropy, and speed of sound, respectively. The notations are used in large letters for the basic flow parameters, but

the small letters are for the corresponding disturbances. All parameters are made nondimensional by using

$$r_0, r_0\sqrt{\rho_\infty}/\sqrt{p_\infty}, \sqrt{p_\infty/\rho_\infty}, p_\infty, \rho_\infty$$

as scales for length, time, velocity, pressure, and density respectively, with r_0 being a characteristic core radius. The infinity subscript denotes the value at infinity.

The flow to be studied is a stationary vortex whose parameters do not depend on the polar angle ϕ and radial velocity is zero. Other flow parameters must satisfy the following relation:

$$\frac{dP}{dr} = \frac{RV^2}{r}, \quad S = \ln P/R^\gamma \quad (1)$$

which can be integrated providing that distributions of two parameters in the radial direction are known, e.g., $V = V(r)$ and $S = S(r)$. Here S is the relative entropy, i.e., $S - S_\infty$.

The linear-stability analysis is applied to this flow, which considers the behavior of an infinitesimal disturbance superposed on the basic flow. The disturbance is analyzed into normal modes, when all parameters have a similar (t, ϕ) -dependence given by $\exp[i(\lambda t + m\phi)]$, with λ and m being a constant, generally complex, and a positive integer, respectively, e.g.,

$$p(t, r, \phi) = p(r) \exp[i(\lambda t + m\phi)] \quad (2)$$

By introducing new variables ξ and η related to the velocity components u and v as

$$u = \frac{i\sigma\xi}{R}, \quad v = -\frac{1}{R} \left[i\sigma\eta - r \frac{d(\Omega)}{dr} \xi \right] \quad (3)$$

which can be treated as an analog of the Lagrangian displacement introduced [7] for the circular flow of an incompressible fluid, and eliminating the amplitudes $\eta(r)$, $\rho(r)$, and $s(r)$, the resulted system of linearized equations can be represented by two differential equations for the amplitudes $p(r)$ and $\xi(r)$:

$$\begin{aligned} \frac{dp}{dr} &= \left(\frac{2m}{r\sigma} \Omega - \frac{r\Omega^2}{C^2} \right) p - (\sigma^2 - \Phi) \xi \\ \frac{1}{r} \frac{d(r\xi)}{dr} &= \left(\frac{m^2}{r^2\sigma^2} - \frac{1}{C^2} \right) p + \left(\frac{2m}{r\sigma} \Omega - E \right) \xi \end{aligned} \quad (4)$$

where $\Omega = V/r$ and $C = \sqrt{\gamma P/R}$ are the local angular velocity the speed of sound of the basic flow,

$$\Phi = \frac{2\Omega}{r} \frac{d(r^2\Omega)}{dr} - r\Omega^2 E, \quad E = \frac{1}{\gamma} C^2 \frac{dS}{dr} \quad (5)$$

and $\sigma = \lambda + m\Omega$ is the Doppler-shifted frequency.

Eqs. (4) must be solved for all domain $0 \leq r \leq +\infty$ under the boundary condition

$$\xi = 0 \quad \text{for } r = 0 \quad (6)$$

Another condition is that the solution must remain bounded, i.e.,

$$|\xi|, |p| \leq M < +\infty \quad \text{for all } r, \quad 0 \leq r \leq +\infty \quad (7)$$

with M being a positive constant. Taking a positive integer for m , Eqs. (4)-(7) define an eigenvalue problem for λ , which is generally complex. Its real part, $\lambda_r = \text{Re}(\lambda)$, represents the azimuthal phase frequency, while the imaginary part, $\lambda_i = \text{Im}(\lambda)$, gives the temporal growth rate.

Note that neither the equations nor the boundary conditions involve any complex unit i . Therefore, the spectrum of eigenvalues must be symmetrical with respect to the real axis. To each decaying mode there must be a corresponding growing mode. Hence, existing complex eigenvalues ensures the instability of the basic vortex flow.

2.2 Basic vortex flow

We assume that the basic vortex is homentropic, i.e., $S(r) = 0$, and isolated, with the azimuthal velocity profile defined by the steepness parameter β in the similar way as it was proposed in [3]:

$$V(r) = \mu r \exp(-r^\beta) \quad (8)$$

where μ characterizes the strength of the vortex and equals the non-dimensional angular velocity of gas rotation in the vicinity of the vortex center. For the foregoing, E in Eq. (4) vanishes and the sound velocity squared acquires the following profile:

$$C^2(r) = \gamma - \frac{\gamma-1}{\beta} \left(\frac{1}{2} \right)^{2/\beta} \mu^2 \Gamma \left(\frac{2}{\beta}, 2r^\beta \right) \quad (9)$$

where $\Gamma(a, x)$ is the incomplete Gamma function.

The pressure and density profiles of the basic flow are defined, respectively, by

$$P(r) = \left[\frac{1}{\gamma} C^2 \right]^{\frac{\gamma}{\gamma-1}}, \quad R(r) = \left[\frac{1}{\gamma} C^2 \right]^{\frac{1}{\gamma-1}} \quad (10)$$

The condition $C^2 \geq 0$ imposes the following restriction on the vortex parameters:

$$\mu^2 \leq \frac{\gamma}{\gamma-1} 2^{2/\beta} \frac{\beta}{\Gamma(2/\beta, 0)} \quad (11)$$

As the strength increases, the pressure in the vortex lowers until it reaches zero at the center. Further increase in strength beyond the limit of Eq. (11) leads to the regime when gas evacuates the vicinity of the center. This regime is beyond the scope of the present study and is not considered here.

2.3 Boundary conditions and far field asymptotics

As $r \rightarrow 0$, the angular velocity Ω approaches the value μ , and the asymptotic solution is given by

$$\xi = \xi_* m r^{m-1}, \quad p = \xi_* \sigma_0 (\sigma_0 - 2\mu) r^m \quad (12)$$

where $\sigma_0 = \lambda + m\mu$ and ξ_* is a constant that can be chosen arbitrarily.

We will study only the cases $m \geq 2$. The axisymmetric mode $m = 0$ has been investigated in [8]. When $m = 1$, no non-trivial solutions exist that satisfy both Eq. (4) and the condition of zero velocity at the origin, and therefore the $m = 1$ mode cannot be realized.

The asymptotic solution for $r \rightarrow +\infty$ is given by the Hankel function $H_m^{(2)}$ as

$$\begin{aligned} p(r) &= p_* H_m^{(2)}(\zeta) \\ \xi(r) &= \frac{p_*}{\lambda C_\infty} \left[H_{m-1}^{(2)}(\zeta) - \frac{m}{\zeta} H_m^{(2)}(\zeta) \right] \end{aligned} \quad (13)$$

where $\zeta = \lambda r / C_\infty$, p_* is the constant that depends on the choice of the constant ξ_* in the asymptotic solution for $r \rightarrow 0$. In Eq. 13 we consider only the eigenvalues that have negative imaginary

parts, $Im(\lambda) < 0$. For complex conjugate eigenvalues with $Im(\lambda) > 0$, corresponding temporally decaying modes, the solution is given by the Hankel function $H_m^{(1)}$, which describes inward-going waves.

The asymptotics of Eq. (13) represents outward going waves. Using the asymptotic behavior of the Hankel function at infinity

$$H_m^{(2)}(z) \approx \sqrt{\frac{2}{\pi z}} \exp \left[-i \left(z - \frac{1}{2} m \pi - \frac{1}{4} \pi \right) \right]$$

for $-2\pi \leq \arg z < \pi$, the disturbance pressure in the far field can be written as

$$p(r, \varphi, t) \approx \sqrt{\frac{2}{\pi r}} \left(\frac{C_\infty}{\lambda_i^2 + \lambda_r^2} \right)^{\frac{1}{4}} \exp(\lambda_i t^*) \cdot \exp[-i(\lambda_r t^* + \psi - m\varphi)]$$

where $t^* = r/C_\infty - t$ is the retarded time and $\psi = 0.5 \arg \lambda - 0.75\pi - 0.5m\pi$ is the phase shift. Thus, unstable eigenfunctions in the far field resemble spiral out-going sound waves with the circular frequency given by the real part of the eigenvalue λ_r . The wave length δ (the distance between 2 convolutions of the spiral) is also determined by λ_r and given by $\delta = 2\pi m C_\infty / \lambda_r$.

2.4 Solution of the eigenvalue problem

Eliminating p_* in Eq. 13 yields the following asymptotic relation between ξ - and p -amplitudes as $r \rightarrow +\infty$:

$$\begin{aligned} \lambda C_\infty H_m^{(2)}(\zeta) \xi(r) &= \\ \left[H_{m-1}^{(2)}(\zeta) - \frac{m}{\zeta} H_m^{(2)}(\zeta) \right] p(r) \end{aligned} \quad (14)$$

The calculation of the complex eigenvalue λ can then be fulfilled by solving Eq. (4) as an initial-value problem with Eq. (12) applied at some small $r = r_{00}$. The iteration parameter is the eigenvalue λ which is varied until the solution satisfies the asymptotic relation given by Eq. (14) at a large $r = r_\infty$. The calculation is started with $r_\infty = 3$. The convergence in λ is typically achieved at the value of $r_\infty \approx 5$.

This approach is realized with the use of the *MATLAB*, a software for mathematical computing. The calculation is performed with the *MATLAB*'s program *bvp4c* that solves differential equations subject to general, two-point boundary conditions involving a vector of unknown parameters. With this program, the eigenvalue problem is solved on a sequence of intervals $[r_{00}, r_{\infty}]$ with different, gradually increasing values of r_{∞} until the eigenvalue λ converges.

2.5 Results: eigenvalues and eigenfunctions

This section presents some results of working the eigenvalue problem formulated in the previous sections. We start with the $m = 2$ mode. The calculated eigenvalues are shown in Fig. 2 as functions of the vortex intensity μ for several different values of the steepness β . We draw only those eigenvalues that have negative imaginary parts; the complex conjugate eigenvalues are not given because they correspond to temporally decaying modes, which describe inward-going waves.

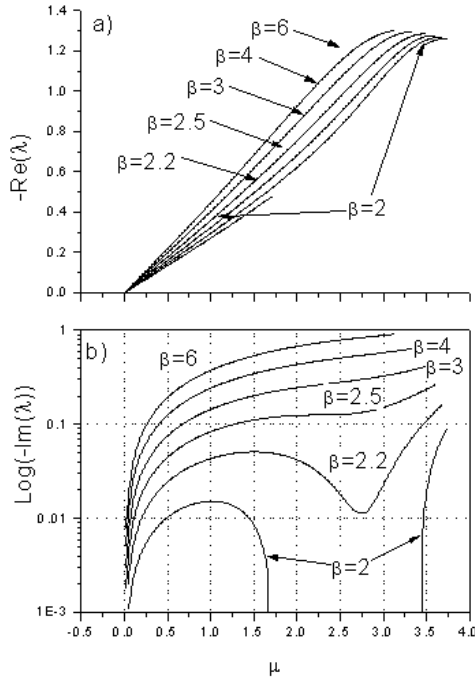


Fig. 2 Eigenvalue of the $m = 2$ mode versus μ .

The lower part of Fig. 2 displays the imaginary part that represents the growth rate of dis-

turbances while the upper one the real part that is proportional to the phase angular velocity (the latter is equal to $-\lambda_r/m$).

The instability of the vortex is strongly dependent on the steepness of the peripheral region of opposite vorticity; as steeper this region as stronger the instability. Also, one can see that weak vortices with smaller intensities μ are unstable at any positive steepness. However this instability is rather weak. The growth rate is rising with increasing of μ . But the further behavior depends on the steepness. For moderate values ($\beta < \text{or} \sim 2.2$), the growth rate reaches a maximum and then rapidly decreases so that the vortex can even fall into a stable state at a certain intensity and remains stable at all higher intensities almost up to the limit (evacuation) intensity; only highly-intensive vortices, nearly evacuated, again become unstable. Vortices of a higher steepness ($\beta > 2.5$) are unstable at all intensities, with instability becoming stronger as the intensity strengthens.

The behavior of the real part of eigenvalues against μ is nearly linear for all β . It is convenient to normalize the phase velocity by the angular velocity of the basic vortex that is represented by μ . Thus, the parameter $-\lambda_r/(m\mu)$ defines how fast the angular phase velocity is with respect to the basic vortex angular velocity. One can see, that independently on the velocity profile in the basic vortex this parameter is roughly 0.2, the angular phase velocity is roughly 5 times slowly than the speed of the vortex rotation.

Eigenvalues for higher modes are shown in Figs. 3 ($m = 3$) and 4 ($m = 4$). One can see that the instability of these modes becomes stronger (the growth rate rises) as the vortex intensity increases. However, unlike the $m = 2$ mode case, it peaks at a certain intensity and after that quickly descends. Therefore, most of strong isolated vortices appear to be stable with respect to higher modes; only those with a large steepness ($\beta \sim \text{or} > 6$) still remain unstable to the $m = 3$ modes over the all range of intensities.

The real part of eigenvalues for higher modes is about linear function with μ and only slightly depends on the steepness. The slopes are ≈ 0.75

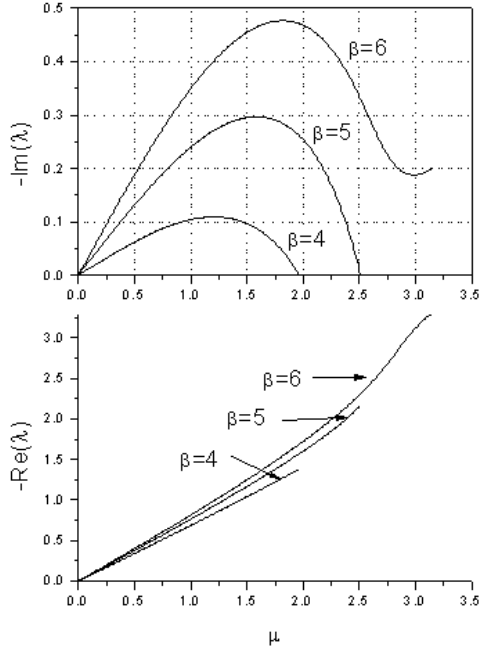


Fig. 3 Eigenvalue of the $m = 3$ mode versus μ .

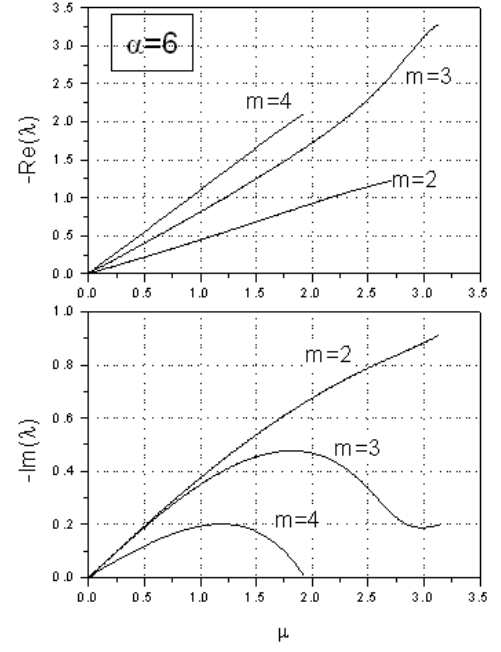


Fig. 5 Comparison between eigenvalues for the $m = 2, 3$, and 4 modes; $\beta = 6$.

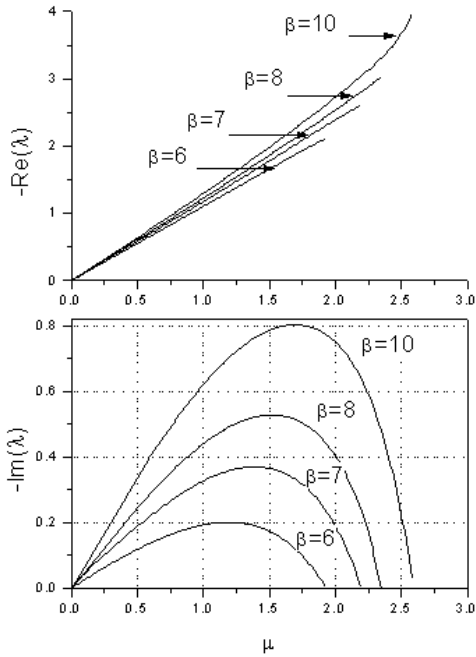


Fig. 4 Eigenvalue of the $m = 4$ mode versus μ .

and ≈ 1.2 for $m = 3$ and $m = 4$, respectively. Thus, the azimuthal phase velocity is about a quarter (for $m = 3$) and a third (for $m = 4$) of the vortex angular velocity.

For comparison, the eigenvalues for differ-

ent modes are presented in Fig. 5. The eigenvalue is given versus intensity for the case $\beta = 6$. Typically, the higher the mode of disturbances is the weaker their instability (smaller growth rate). One can also note that the growth rates of $m = 2$ and $m = 3$ modes are almost coincides for weak vortices with $\mu \leq 0.5$.

Finally, we describe typical patterns of eigenfunctions. A common feature of the disturbance pattern is the set of alternating eddies (4 for $m = 2$, 6 for $m = 3$, and 8 for $m = 4$) located at the periphery of the basic vortex. These eddies form an eddy wave that travels in the azimuthal direction with the angular phase velocity equal $-\text{Re}(\lambda)/m$. The eddies that are co-rotating with the basic vortex produce a higher pressure (positive values of the disturbance pressure), while those counter-rotating a lower (negative) pressure. Thus, the instability shows itself as an eddy wave in the vortex periphery, where constituent eddies roll over the core in the direction of the vortex rotation.

3 Non-linear stage

In this section we deal with the non-linear stage of the evolution of instabilities in the isolated vortex considered in the previous section. This study is conducted by numerically solving the unsteady compressible two-dimensional Navier-Stokes equations.

The initial distribution of flow parameters are taken in the form of the basic isolated homentropic vortex, on which a small disturbance is superimposed in the form of normal mode. The disturbance pressure amplitude is 10^{-5} of the basic pressure at infinity.

The basic computational domain is a square with a non-dimensional length of 6, which is surrounded by outflow boundary zones extended by a length of 20. The boundary zones are involved in the calculation to absorb outgoing disturbances with minimal reflection. The grid of the basic domain consists of 400 cells uniformly distributed in each direction. The equations are discretized in space with the Godunov method implemented by the third order accurate MUSCL-type interpolation ([9], [10]). The time integration is performed with the third order accurate Runge-Kutta scheme.

3.1 The $m = 2$ mode instability

First, we consider the development of the $m = 2$ normal mode superimposed on the vortex with $\mu = 0.5$ and $\beta = 6$. Instantaneous flow patterns are given by the velocity vector field for several time instants in Figs. 6-8. The time is given in T_{rot} that is the period of one basic vortex rotation ($\mu/(2\pi)$).

The characteristic time of the linear stage for the considered conditions is defined by $-1/Im(\lambda)$ and equals to 5.2 or $0.4T_{rot}$. Therefore, the first instant presented in Fig. 6 corresponds to the linear stage: disturbances have grown by one order, but are not still seen on the background of the basic flow. The next instant, $2.87T_{rot}$, is that when disturbances have been sufficiently developed to modify the basic flow; the vortex acquires an oval shape. Also, two small

counter-rotating secondary eddies can be seen in the periphery.

The following two snapshots illustrate the process of vortex breakdown. The vortex is stretched with forming two counter-rotating eddies (time= $3.82T_{rot}$) that gradually recede from the origin (time= $4.78T_{rot}$).

The instant $5.73T_{rot}$ shows the formation of small secondary eddies orbiting nearby the primary those. These primary and secondary eddies make two pairs of counter-rotating eddies. The further motion of the pairs is defined by the interaction between these eddies: the pairs recede each other (time= $8.60T_{rot}$) and then approach (time= $11.46T_{rot}$). At the maximal approach (time= $13.38T_{rot}$) they rotate at an angle (time= $15.23T_{rot}$), and then again recede (time= $19.10T_{rot}$), and so on. Thus, the vortex breakdown result in the formation of two pairs of counter-rotating eddies that orbit the center of the original vortex, periodically receding from (time= $19.10T_{rot}$) and approaching to it (time= $24.83T_{rot}$).

3.2 The $m = 3$ mode instability

Figs. 9 and 10 show successive instants of the evolution of the $m = 3$ disturbance mode superimposed on the vortex with $\mu = 0.5$ and $\beta = 6$. For this mode, $Im(\lambda) = -0.19$ so that the characteristic time of the linear stage is nearly the same as for the case $m = 2$, 5.3 or $0.42T_{rot}$.

This evolution differs from that of the $m = 2$ mode described in the previous section. The non-linear stage is appeared after the basic vortex executes 1 – 2 rotations. At time= $3.82T_{rot}$ the basic vortex is compressed by 3 counter-rotating eddies and acquires a typical triangle-type shape. Unlike the $m = 2$ case, this flow pattern does not destroyed and remains for a long time; yet at time= $7.64T_{rot}$ one still can see the similar pattern. However, by this instant the position of the counter-rotating eddies is slightly asymmetrical. One revolution after that (time= $8.60T_{rot}$), two of the three eddies merge, and we can see a flow pattern with only two secondary eddies, similar to that observed for the $m = 2$ case.

From this instant, the process of vortex breakdown begins: the two secondary eddies stretch the basic vortex ($\text{time}=9.55T_{rot}$) and tear it in half. As this takes place, two pairs of counter-rotating eddies are formed ($\text{time}=11.46T_{rot}$). However, these pairs are asymmetrical with respect the center, and move independently each to other as seen for the instant $14.32T_{rot}$.

References

- [1] A. Michalke and A. Timme. On the inviscid instability of certain two-dimensional vortex-type flows. *J. Fluid Mech.* **29**, Vol. 4, 647 (1967).
- [2] F. Bottausci and P. Petitjeans. Visualization of stretched vortices. In *Vortex Structure and Dynamics, Lecture Notes in Physics*, edited by A. Maurel and P. Petitjeans (Springer, Berlin, 1999), pp. 124-134.
- [3] X. Carton and J. McWilliams. Barotropic and baroclinic instabilities of axisymmetric vortices in a quasi-geostrophic model. In *Mesoscale/Synoptic Coherent Structures in Geophysical Turbulence*, edited by J. Nihoul and B. Jamart (Elsevier, New York, 1989), pp. 225-244.
- [4] G. Flierl. On the instability of geostrophic vortices. *J. Fluid Mech.* **197**, 349 (1988).
- [5] J.-M. Ghomaz, M. Rabaud, C. Basdevant, and Y. Couder. Experimental and numerical investigation of a forced circular shear layer, *J. Fluid Mech.* **187**, 115 (1988).
- [6] F. Gallaire and J.-M. Chomaz. Three-dimensional instability of isolated vortices. *Phys. Fluids.* **15**, 2113 (2003).
- [7] S. Chandrasekhar. *Hydrodynamic and hydro-magnetic stability*. (Dover Publications, INC, New York, 1954), pp.277-284.
- [8] L. N. Howard. On the stability of compressible swirling flow. *Stud. Appl. Maths.* **52**, 39 (1973).
- [9] S. K. Godunov. A difference scheme for numerical computation of discontinuous solution of hydrodynamic equations. *Math.sb.* **47**, 271 (1959).
- [10] B. van Leer. Toward the ultimate conservative difference scheme, II. *J. Comput. Phys.* **14**, 361 (1979).

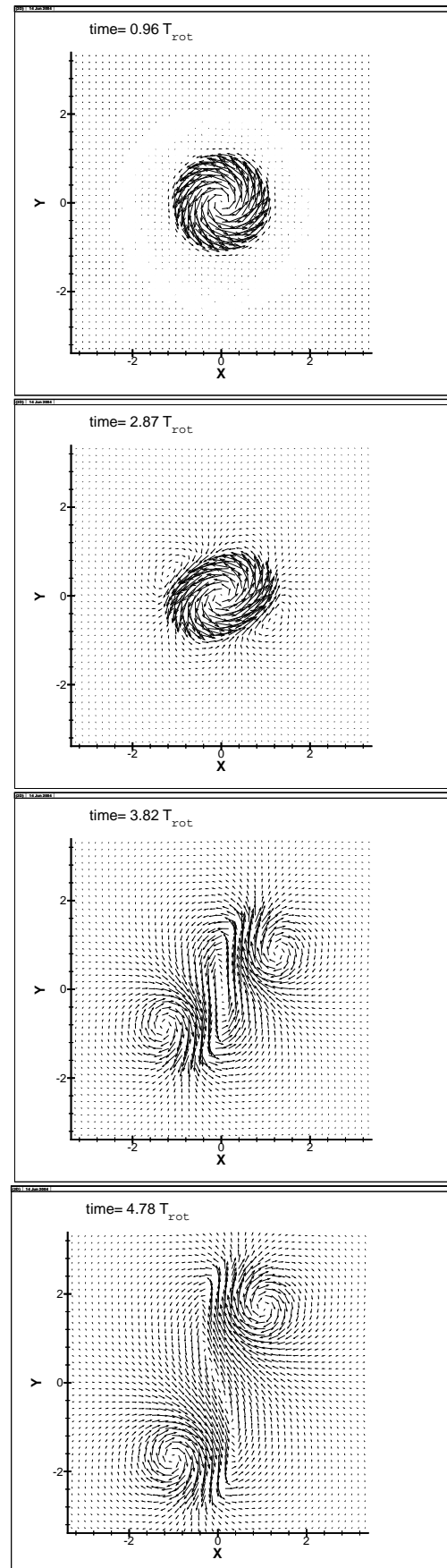


Fig. 6 (continued: see caption to Fig. 8)

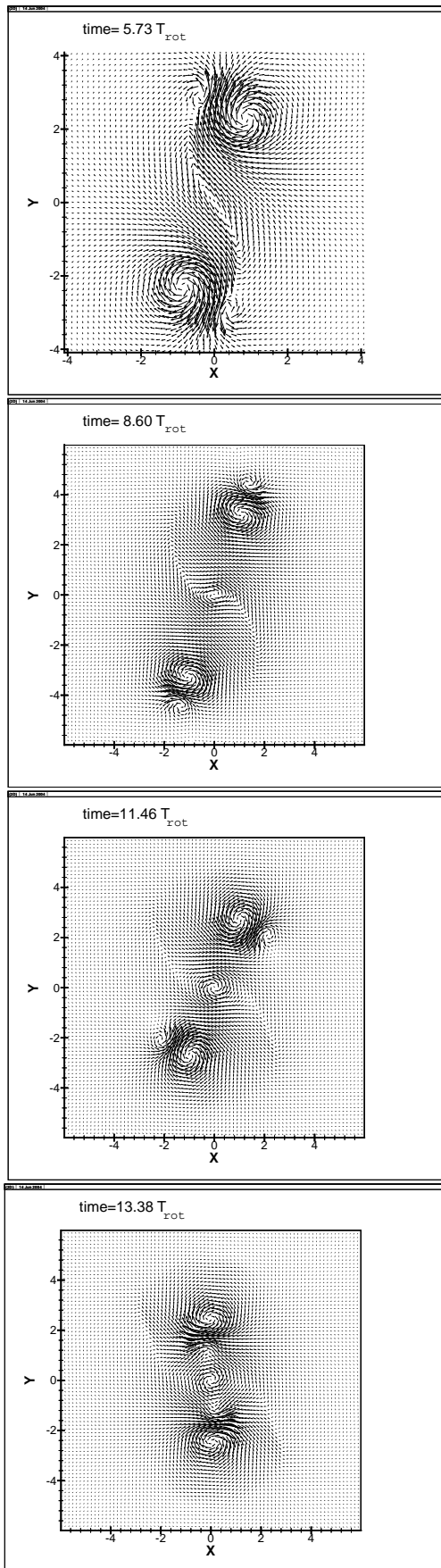


Fig. 7 (continued:see caption to Fig. 8)

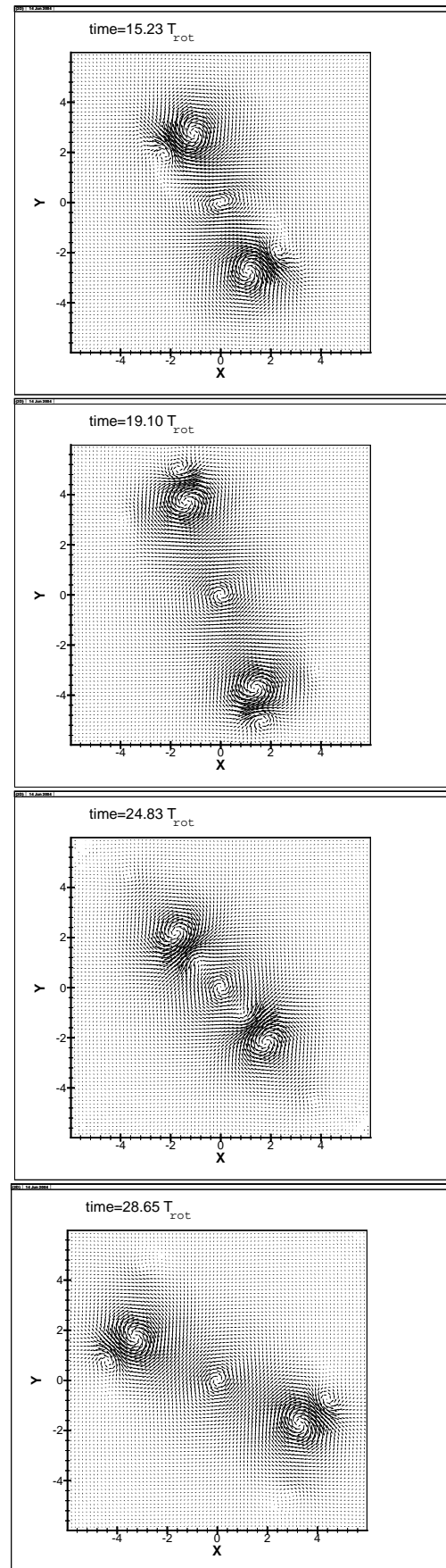


Fig. 8 Non-linear evolution of the vortex disturbed by the $m = 2$ mode eigenfunctions ($\beta = 6$ and $\mu = 0.5$)

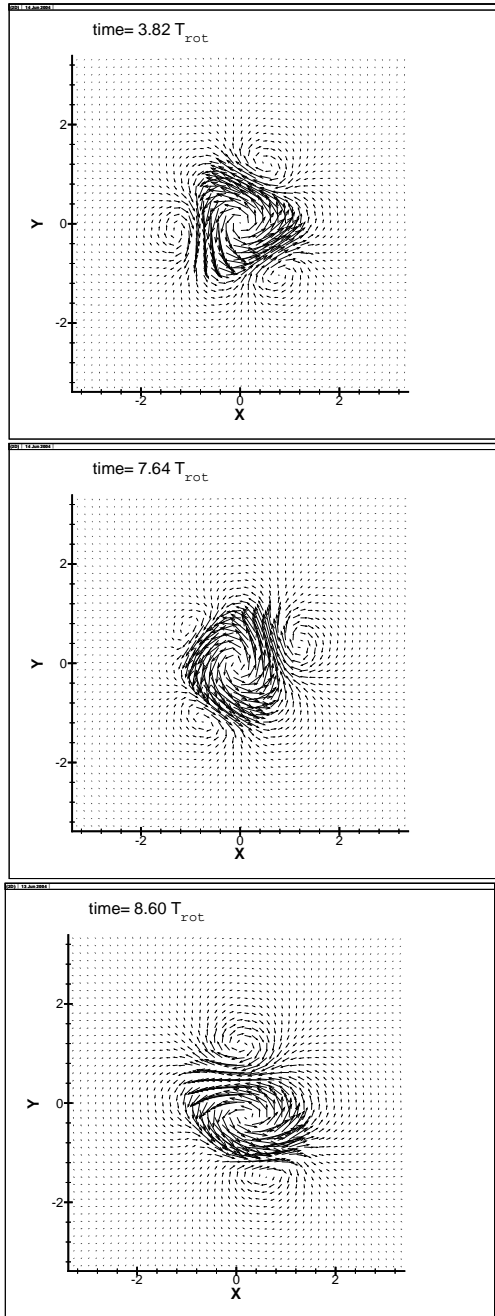


Fig. 9 (continued:see caption to Fig. 10)

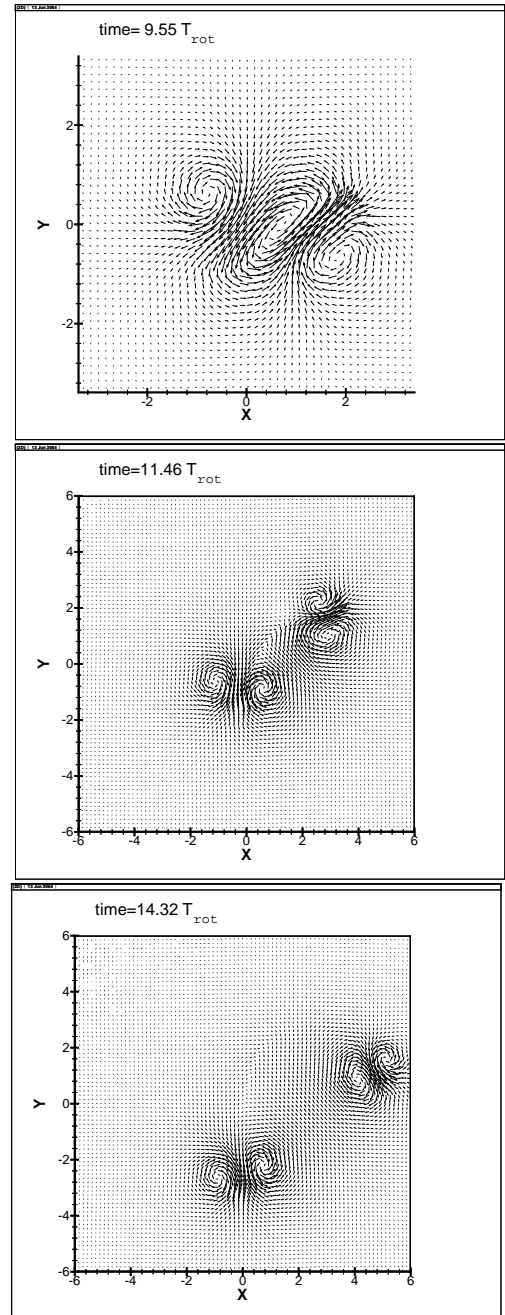


Fig. 10 Non-linear evolution of the vortex disturbed by the $m = 3$ mode eigenfunctions ($\beta = 6$ and $\mu = 0.5$)